RSC Advances

PAPER

View Article Online
View Journal | View Issue

Cite this: *RSC Adv.*, 2022, **12**, 21340

Synthesis, antitumor activity, 3D-QSAR and molecular docking studies of new iodinated 4-(3*H*)-quinazolinones 3*N*-substituted†

Marcia Pérez-Fehrmann, *[a] Víctor Kesternich, [a] Arturo Puelles,[a] Víctor Quezada, [a] Fernanda Salazar,[a] Philippe Christen, [bc] Jonathan Castillo,[d] Juan Guillermo Cárcamo,[de] Alejandro Castro-Alvarez [fg] and Ronald Nelson *[a]

A novel series of 6-iodo-2-methylquinazolin-4-(3*H*)-one derivatives, **3a–n**, were synthesized and evaluated for their *in vitro* cytotoxic activity. Compounds **3a**, **3b**, **3d**, **3e**, and **3h** showed remarkable cytotoxic activity on specific human cancer cell lines when compared to the anti-cancer drug, paclitaxel. Compound **3a** was found to be particularly effective on promyelocytic leukaemia HL60 and non-Hodgkin lymphoma U937, with IC_{50} values of 21 and 30 μM, respectively. Compound **3d** showed significant activity against cervical cancer HeLa (IC_{50} = 10 μM). The compounds **3e** and **3h** were strongly active against glioblastoma multiform tumour T98G, with IC_{50} values of 12 and 22 μM, respectively. These five compounds showed an interesting cytotoxic activity on four human cancer cell types of high incidence. The molecular docking results reveal a good correlation between experimental activity and calculated binding affinity on dihydrofolate reductase (DHFR). Docking studies proved **3d** as the most potent compound. In addition, the three-dimensional quantitative structure–activity relationship (3D-QSAR) analysis exhibited activities that may indicate the existence of electron-withdrawing and lipophilic groups at the *para*-position of the phenyl ring and hydrophobic interactions of the quinazolinic ring in the DHFR active site.

Received 14th June 2022
Accepted 19th July 2022

DOI: 10.1039/d2ra03684c

rsc.li/rsc-advances

1 Introduction

4-(3*H*)-Quinazolinones are an important group of fused heterocycles found in interesting natural alkaloids and drugs (Fig. 1). These structures are of high interest due to their wide range of biological and pharmacological properties,[1] including antibacterial,[2] antifungal,[3] antitubercular,[4] antimalarial,[5] anti-toxoplasma,[6] anti-inflammatory,[7] anti-ulcer,[8] and kinase inhibitor,[9] and anticancer activities.[10] Quinazolines as anticancer agents have received considerable attention since the development of the thymidylate synthetase inhibitors altitrexed and thymitaq.[11] Since then, several quinazolines have been described with anticancer activity,[10] among which the following can be highlighted: inhibitors of epidermal growth factor receptor (EGFR),[12] inhibitors of angiogenesis by inhibiting the vascular endothelial growth factor receptor (VEGFR-2)[13] and dihydrofolate reductase (DHFR) inhibitors that prevent the

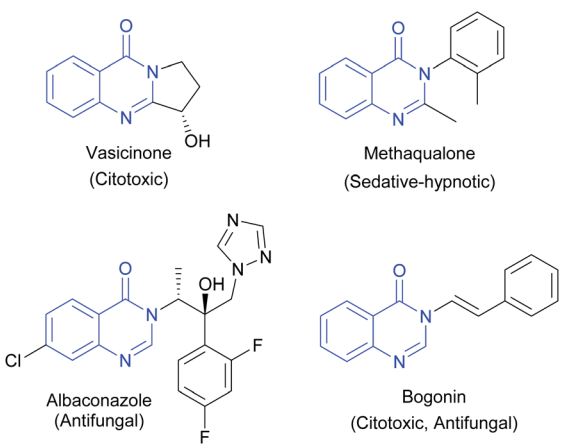

Fig. 1 Selected examples of 4-(3*H*)-quinazolinones.

[a]*Departamento de Química, Facultad de Ciencias, Universidad Católica del Norte, Av. Angamos 0610, Antofagasta 1270709, Chile. E-mail: rnelson@ucn.cl*

[b]*School of Pharmaceutical Sciences, University of Geneva, 1211 Geneva 4, Switzerland*

[c]*Institute of Pharmaceutical Sciences of Western Switzerland, University of Geneva, 1211 Geneva 4, Switzerland*

[d]*Instituto de Bioquímica y Microbiología, Facultad de Ciencias, Universidad Austral de Chile, Campus Isla Teja, Valdivia, Chile*

[e]*Centro FONDAP, Interdisciplinary Center for Aquaculture Research (INCAR), Chile*

[f]*Laboratorio de Bioproductos Farmacéuticos y Cosméticos, Centro de Excelencia en Medicina Traslacional, Facultad de Medicina, Universidad de La Frontera, Av. Francisco Salazar 01145, Temuco, 4780000, Chile*

[g]*Departamento de Química de los Materiales, Facultad de Química y Biología, Universidad de Santiago de Chile, Casilla 40, Correo 33, Santiago, Chile*

† Electronic supplementary information (ESI) available. See https://doi.org/10.1039/d2ra03684c

growth of cancer cells and depletes the cell from thymine causing cell death.[14] Consequently, DHFR inhibition played an essential role in medicine clinical as antitumor agents and becomes a target for the development of new antitumor agents.[15]

Additionally, they are important intermediates in natural product preparation and are used as structural scaffolds in drug discovery.[16] Due to the extensive biological properties associated with quinazolinone moieties in drug design, obtaining these compounds is of great relevance and has motivated the development of multiple synthetic strategies such as ring opening of isatoic anhydride by nitrogen nucleophiles followed by the oxidative cyclocondensation by electrophiles,[17] aza-Wittig/cyclization reactions of iminophosporanes,[18] oxidative olefin bond cleavage,[19] transition metal dehydrogenative coupling,[20] transition metal-free dehydrogenative coupling,[21] transition metal-catalyzed cross-coupling,[22] palladium-catalyzed carbonylative methods[23] and miscellaneous transition metal-free methods.[24] Likewise, interest in these compounds has also led to spectroscopic structural studies, and X-ray diffraction analysis of this class of heterocycles.[25]

Here we report the synthesis of novel 6-iodo-2-methylquinazolin-4-(3*H*)-one derivatives (**3a–n**), carrying different substituents in the 3*N* position. The cytotoxic activity of these new derivatives against various cancer cell lines was evaluated *in vitro*, and molecular docking and 3D-QSAR studies of the compounds were completed to correlate the structures with their cytotoxic activities. The IC_{50} values obtained for the derivatives were contrasted with those obtained with paclitaxel, a chemotherapy drug used to treat many different types of cancer. The objective of forming these compounds is to develop an active antitumor agent with potential activity and selectivity toward human cancer cells *in vivo*.

The synthesis of iodine quinazolinones was developed because iodinated derivatives are characterized as stable, non-toxic, and relatively easy to obtain.[26,27] Previous work has shown that the atom in position six increases lipophilicity and molecular absorption.[27,28] On the other hand, iodinated compounds offer an interesting starting point for the realization of various synthetized analogues.[29]

2 Results and discussion

2.1 Chemistry

For the synthesis of the quinazolinones 3*N*-substituted obtained in the present work, many reactions were tested.[30] However, the method described by Grimmel *et al.*,[31] allowed us to achieve better yields. Thus, the synthesis of 6-iodo-2-methylquinazolin-4-(3*H*)-one 3*N*-substituted were carried out using the 5-iodoanthranilic acid (**1**) as key intermediate. The iodination of anthranilic acid in presence of hydrogen peroxide in ethanol at reflux, gave the compound **1** with 88% yield. Then, the reaction of acid **1** with acetic anhydride and subsequent hydrolysis under reflux, it was possible to obtain 2-acetamido-5-iodobenzoic acid (**2**) in with 75% yield (Scheme 1). Finally, the reaction of intermediate **2** with different amine derivatives (R-NH_2) in the presence of PCl_3 as dehydrating agent, allowed us to obtain the quinazolinones **3a–n** with variated yields (Scheme 2).

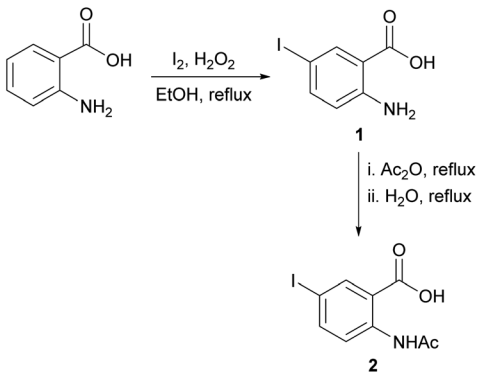

Scheme 1 Synthesis of 2-acetamido-5-iodobenzoic acid (**2**).

As can be seen from Scheme 2, the lowest yield occurred in the synthesis of compound **3n** (21%). It seems that the presence of a nitro group in the *ortho* position of the phenyl ring has an unfavourable effect on the reactivity because this behaviour was not observed when obtaining compounds **3g** (*p*-NO_2) and **3j** (*m*-NO_2), with respective yields of 61 and 65%. On the other hand, the highest yields were obtained in the synthesis of **3h** (*m*-Cl-*p*-F) and **3i** (hydrazine derivative), both with 80% yields.

The structures of quinazolinones **3a–n** was confirmed by IR, ^{1}H NMR, ^{13}C NMR-APT, and high-resolution electrospray-ionisation mass spectrometry (HRESIMS) methods. In general, the IR spectra of all compounds showed a C=O stretching band in the 1652–1685 cm^{-1} range, as well as a C=N stretching band of the quinazolinone ring in the 1598–1616 cm^{-1} range. In the ^{1}H NMR spectra, the most characteristic signal was a singlet in the range of $\delta_H = 2.11$–2.45, corresponding to the protons of the methyl group H_{12} at C_2. In the ^{13}C NMR-APT spectra, C=O signals were seen at $\delta_C = 160.3$–158.9. In addition, a chemical shift was seen at $\delta_C = 158.5$–154.2 and 91.8–90.9, corresponding to C_2 and C_6, respectively. These spectroscopic data confirmed the formation of the quinazolinone ring (see the ESI† for details).

2.2 Cytotoxic activity

The cytotoxic activities of quinazolinones **3a–n** were measured using the MTT colorimetric method against six cancer cell lines: G415, Gbd1, T98G, HeLa, HL60, and U937.[32] The IC_{50} values are summarized in Table 1 and compared to paclitaxel as a positive control. The IC_{50} values fall over a wide range of concentrations, from 10 μM to over 200 μM, demonstrating an important variation in the cytotoxicity of the quinazolinones on different cancer cell lines. The cytotoxic effects were cell line dependent. The human cervical adenocarcinoma cell line, HeLa, was sensitive to **3c**, **3d**, **3e**, **3f**, **3g**, **3h**, **3i**, **3k**, and **3n**, with IC_{50} values of 180, 10, 60, 86, 110, 148, 70, 193, and 175 μM, respectively. For all the other quinazolinones, the IC_{50} values were greater than 200 μM. The human glioblastoma cell line T98G was sensitive to **3e** and **3h** and, to a much lesser extent, **3c**, with IC_{50} values of 12, 22, and

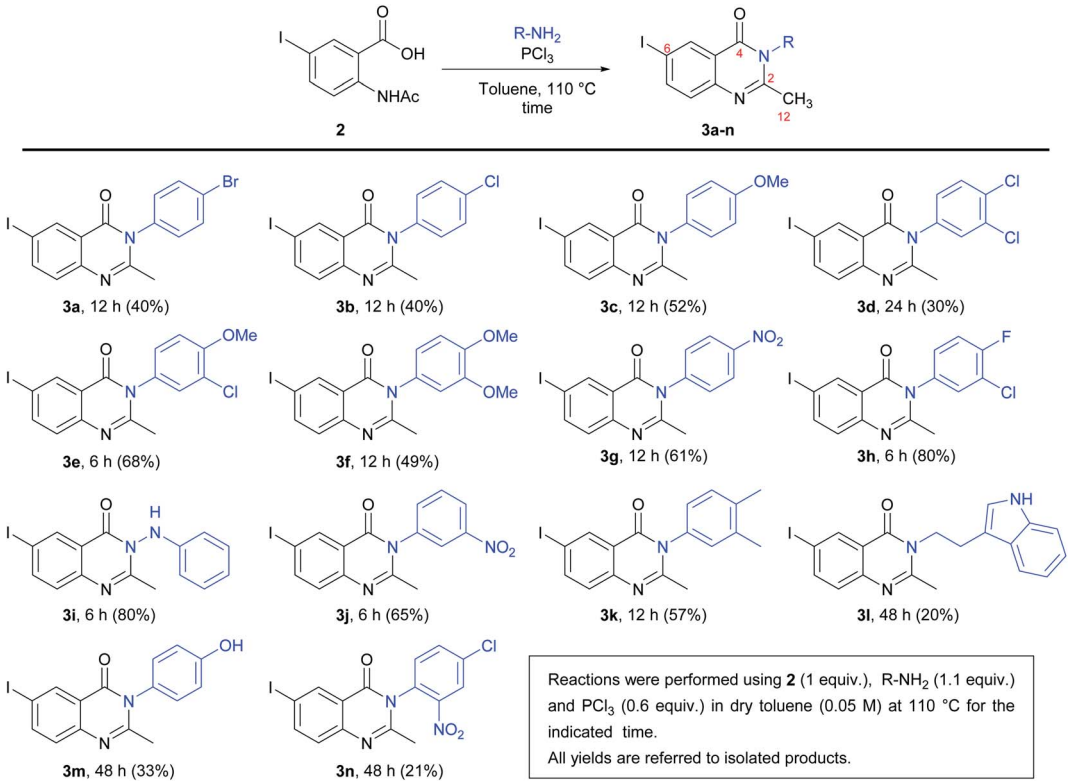

Scheme 2 Synthesis of 6-iodo-2-methylquinazolin-4(3*H*)-one derivatives **3a–n**.

Table 1 Cytotoxic activities of quinazolinone derivatives against the selected cancer cell lines (IC_{50} values expressed in μM)[a]

	Adherent cells			Nonadherent cells		
Comp.	G415	Gbd1	T98G	HeLa	HL60	U937
3a	>200	>200	>200	>200	**21 ± 1.1**	**30 ± 1.5**
3b	>200	>200	>200	>200	**50 ± 0.7**	**58 ± 5.6**
3c	>200	>200	114 ± 22	180 ± 65	>200	>200
3d	>200	>200	>200	**10 ± 0.7**	>200	>200
3e	>200	>200	**12 ± 3.4**	60 ± 1.3	>200	>200
3f	>200	>200	>200	86 ± 12	>200	>200
3g	>200	>200	>200	110 ± 51	>200	>200
3h	>200	>200	**22 ± 1.7**	148 ± 91	>200	>200
3i	>200	>200	>200	70 ± 5.4	>200	>200
3j	>200	>200	>200	>200	>200	>200
3k	>200	>200	>200	193 ± 120	>200	>200
3l	>200	>200	>200	>200	>200	>200
3m	>200	>200	>200	>200	>200	>200
3n	>200	>200	>200	175 ± 98	>200	>200
Paclitaxel	10 ± 0.7	6 ± 0.6	21 ± 3.0	6.2 ± 1.9	3.1 ± 0.9	41 ± 7.0

[a] 50% inhibitory concentration values are an average of three individual experiments.

114 μM, respectively. The human promyelocytic leukemia cell line, HL60, showed a weak sensitivity to compounds **3a** and **3b**, with IC_{50} values of 21 and 50 μM, respectively. The human non-Hodgkin lymphoma cell line, U937, was sensitive to **3a** and **3b**, with IC_{50} values of 30 and 58 μM, respectively. All synthetic compounds were inactive against human gallbladder carcinoma cell lines, G415 and Gbd1 (IC_{50} > 200 μM). Furthermore, compounds **3j–n** were inactive or very weakly active against all cancer cell lines.

From the results summarized in Table 1, it can be deduced that the bromine atom in the *para*-position could be an important factor for the cytotoxicity of compound **3a** against HL60 (IC_{50} = 21 μM) and U937 (IC_{50} = 30 μM) cell lines (Fig. 2). Regarding the inhibitory effect on U937, **3a** showed greater

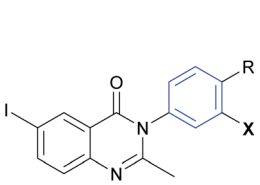

3a: R= Br, X= H; 21 mM (HL-60)
30 mM (U-937)
3b: R= Cl, X= H; 50 mM (HL-60)
58 mM (U-937)
3c: R= OMe, X= H; no active
3d: R= Cl, X= Cl; **10 mM** (HeLa)
3e: R= OMe, X= Cl; **12 mM** (T98G)
3h: R= F, X= Cl; 22 mM (T98G)

Fig. 2 Structures and IC_{50} of-substituted phenyl rings.

cytotoxic activity than paclitaxel ($IC_{50} = 41$ μM). However, when the bromine atom is replaced by a chlorine atom, such as in compound **3b**, the cytotoxic effect over HL60 and U937 decreases with IC_{50} values changing to 50 and 58 μM, respectively. A methoxy group in the *para*-position (compound **3c**) has no cytotoxic activity on these two cell lines. Compound **3d** (*m*,*p*-di-Cl) was very effective on HeLa cells ($IC_{50} = 10$ μM). Compounds **3e** and **3h** showed good efficiency in T98G ($IC_{50} =$ 12 and 22 μM, respectively), considering that paclitaxel showed an IC_{50} value of 21 μM. These three molecules (**3d**, **3e**, and **3h**) have the presence of a chlorine atom in the *meta*-position in common. Other substitutions and analogues studied did not show a promising level of activity in the evaluated cell lines.

2.3 Molecular docking of compound 3d with DHFR

The calculations of molecular docking for model compounds were performed with the aim of elucidating the elements determining the biological activity. The protein selected for docking studies was dihydrofolate reductase (DHFR), which has an important role in the evolution of several human cancers.[33] Moreover, quinazoline and quinazolinone derivatives have been previously described as human DHFR inhibitors.[33] DHFR is an enzyme involved in the synthesis of pyrimidinic base timidin, a structural component of DNA, therefore a molecule that inhibits this enzyme inhibit the DNA synthesis and it can be potentially useful as a drug against several types of cancer.[33] Moreover, as overexpression of DHFR occurs in breast, prostate, gastric/gastroesophageal, ovarian, endometrial, bladder, lung, colon, and head and neck cancers, it is a target for therapies pointing to inhibition of this protein to decrease tumour growth.[34] Principally, the overexpression of this protein is associated in HeLa cell lines.[35]

The molecular docking studies were performed in the active site of DHFR. The results of induced-fit molecular docking, considering flexible residues from 6 Å of the best docked position, describe good correlation among experimental data and calculated values (Fig. 3).

The interaction of synthetized 4-(3*H*)-quinazolinones was observed to get the view of ligand binding modes while docking since a co-crystal ligand was absent for DFHR. Prediction of the size and spatial orientation of the ligand binding sites of proteins was a major challenge due to the small size of the ligand. The active site of the DFHR crystal structure reported in literature was characterized.[36] The important interactions are between residue R71 with an iodine atom, and van der Waals interactions are predominant with amino acids L23, L68, and

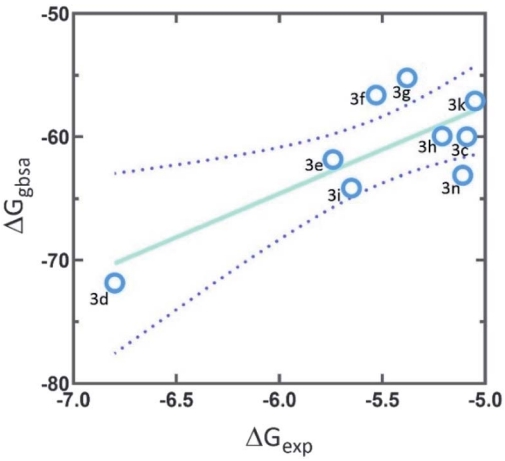

Fig. 3 The correlation graph between experimental activity (ΔG_{exp}) and predicted docking activity (ΔG_{gbsa}).

T57, especially π-stacking with residues F32 and F35 with the quinazolinic aromatic ring (Fig. 4). Altogether, the molecular docking result is in accordance with the binding mechanism of natural ligands (DHF and NADPH), inhibiting catalytic activity of the protein.

2.4 3D-QSAR study

Our first challenge was to understand the small structural differences of these synthetized compounds with their notorious biological activity in distinct cell lines, principally in the HeLa cell line. Therefore, we used a ligand set from Pathak's article.[37] The Pathak's compounds have quinazoline fragments, similar to our synthetized compounds. Alignments of the 24 structures (9 synthetized compounds and 15 compounds of Pathak, see Fig. S1 in ESI†) were carried out from the more active compounds. Compound Pathak_**11** has two halogenated-aromatic fragments, so our compounds were aligned, considering this feature (Fig. 5).

The Comparative Molecular Field Analysis (COMFA)[38] is based on 3D-structured features of molecules, such as electrostatic and hydrophobic properties. Indeed, it becomes necessary to develop a QSAR model to predict biological activity before the synthesis of new cytotoxic quinazolinones. The success of 3D-QSAR and molecular docking studies help to understand relationships between the physicochemical properties and biological activity.

These contour maps give us some general insight into the nature of the receptor-ligand binding region. The training set of 18 compounds, COMFA model with five Partial Least Square (PLS) components, was built, and then, the external test set including six compounds was used to evaluate the reliability and applicability of the built model. Statistical quality parameters associated with COMFA models were based on Fractional Factorial Design (FFD) procedures for noise reduction. The COMFA model gave a good cross-validated correlation coefficient (Q^2) for Leave-One-Out (LOO), Leave-Two-Out (LTO), and Leave-Many-Out (LMO) as 0.854, 0.826, and 0.841 respectively,

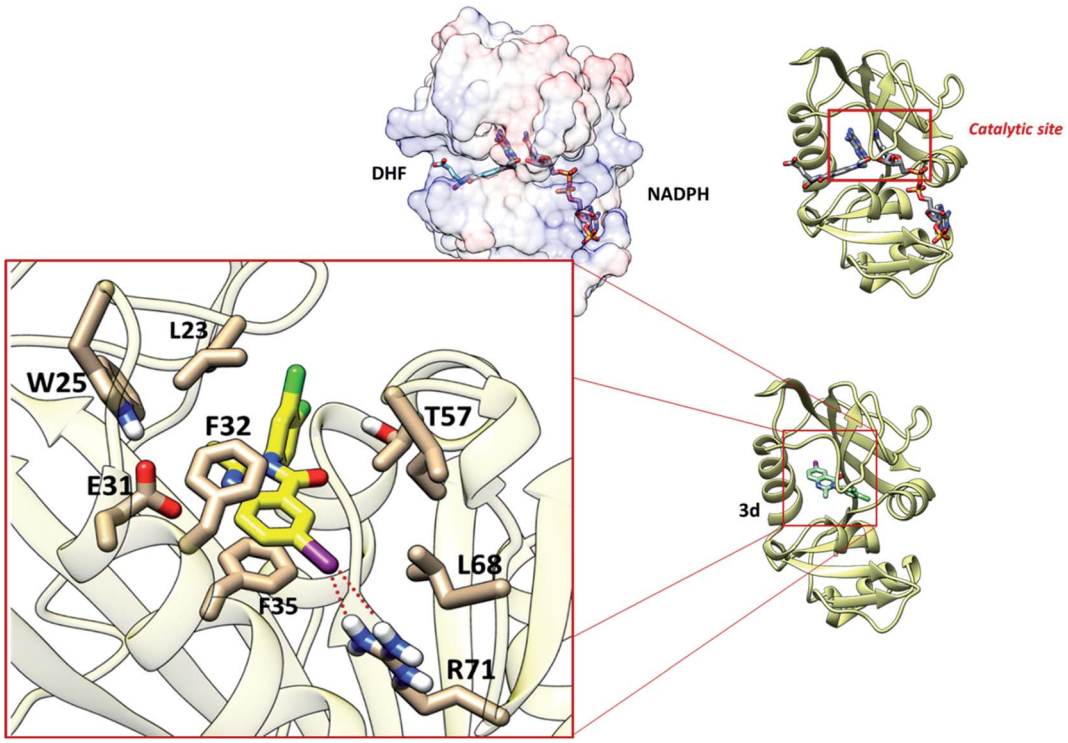

Fig. 4 The binding mode of compound **3d** in the catalytic site of DHFR.

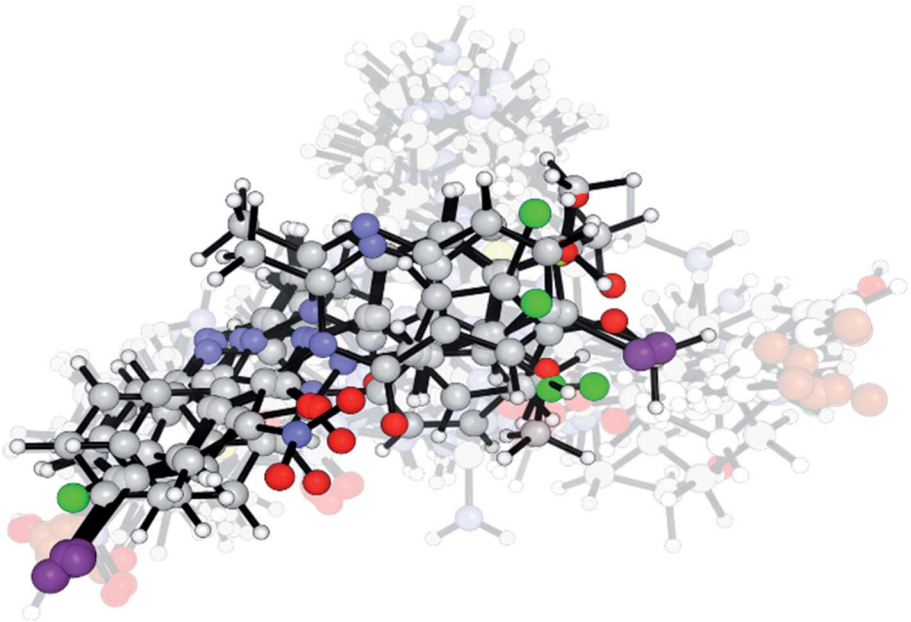

Fig. 5 Aligned structures of all compounds for the 3D-QSAR study. Highlighted structures are synthetized compounds in this work, and transparent structures are from Pathak's dataset.

indicating an excellent internal predictive power of the established model. The PLS analysis with the five components resulted in a conventional R^2 of 0.996, F-test of 666.323, and SDEC of 0.032. Thus, the COMFA model was found to be reasonable (Table 2).

The values of experimental and predicted activities, along with the residual values of the training set and test set molecules, are summarized in Table 3. The scatter plot of the observed *versus* predicted values of pIC_{50} for both the training and test set of COMFA models is shown in Fig. 6. This data shows that the experimental and predicted activities of

Table 2 Statistics of the COMFA models for cytotoxic (HeLA cells) activity[a]

		R^2	SDEC	*F*-test	Q^2	SDEP
Training set	PLS	0.996	0.032	666.323		
	LOO	—	—	—	0.854	0.205
	LTO	—	—	—	0.841	0.2.13
	LMO	—	—	—	0.826	0.146
Test set		0.852				0.210

[a] R^2 = non-cross validated for determination; Q^2 = coefficient of determination for internal validation; SDEC = standard deviation error in calculation; SDEP = standard deviation error in prediction.

Table 3 Data set with experimental activity *versus* calculated activity

Compounds	pIC_{50} exp	pIC_{50} calc	Set
3c	3.745	3.733	Training
3d	5	4.9849	Training
3e	4.222	4.2706	Training
3f	4.066	3.9808	Training
3g	3.959	3.7844	Test
3h	3.83	3.884	Training
3i	4.155	4.1573	Training
3k	3.714	3.8836	Test
3n	3.757	3.7665	Training
Pathak_**1**	5.017	4.8399	Test
Pathak_**2**	5.126	5.1072	Training
Pathak_**3**	4.95	4.969	Training
Pathak_**4**	5.15	5.1361	Training
Pathak_**5**	4.903	5.1317	Test
Pathak_**6**	5.013	5.1289	Test
Pathak_**7**	5.02	5.0128	Training
Pathak_**8**	4.888	5.2175	Test
Pathak_**9**	5.022	5.0288	Training
Pathak_**10**	5.177	5.2045	Training
Pathak_**11**	5.147	5.1017	Training
Pathak_**12**	5.124	5.133	Training
Pathak_**13**	5.142	5.1462	Training
Pathak_**14**	5.075	5.111	Training
Pathak_**15**	4.782	4.7626	Training

inhibitors are very close to each other. This graphical representation, again, confirms the good predictive power of the established model and also indicates that the developed COMFA model is reliable.

Contributions by steric effects are observed mainly in the vicinities of the halogen atom (region (a) in Fig. 7) and C-2 methyl group (region (b) in Fig. 7B), where steric interaction tends to increase activity in these regions. On the other hand, the phenyl ring in position 2 tends to increase activity with a second halogen atom in the *meta* substitution and decrease activity with methoxy/nitro group in *ortho* substitution by a sterically unfavourable interaction, and this, obviously, reduces the activity.

Nevertheless, the electrostatic effects observed are unfavourable interactions around the quinazolinic ring (Fig. 8, red area in region (a)). The electrostatic interaction, with a positive charge on the putative receptor, is favourable for cytotoxic activity, mainly in the vicinity of the aromatic group at position 2.

2.5 Solubility predictions

Physicochemical and pharmacokinetic properties were predicted using the SwissADME Web Service (accessed July 5, 2022) (Table 4). As expected, the synthesized compounds have good liposolubility due to the halogen atoms, essentially the iodine and chlorine atoms, with compound **3d** being the most lipophilic compound with characteristics responsive to the dichlorophenyl group. In contrast, the least lipophilic compounds were compounds **3g** and **3j** (2.55 and 2.57 of consensus log *P*, respectively), which have nitrophenyl structures.[39–41]

The prediction methods of J. Delaney[42] and J. Ali[43] were used to predict water solubility (Table 5), and their results indicate that the synthesized structures have moderate solubility and are soluble in water. The prediction of J. Delaney states that all structures are moderately soluble, while J. Ali suggests that some structures are soluble in an aqueous solvent. Both methods suggest that compound **3d** is moderately soluble in water, as are compounds **3e**, **3h**, **3i**, **3k**, **3l**, and **3n**.

Finally, the drug-likeness of the synthesized compounds was evaluated based on the Lipinski, Ghose, Veber, Egan, and Muegge rules (Table 6), of which the most active compound (**3d**) satisfying all rules except the Lipinski rule; however, compound

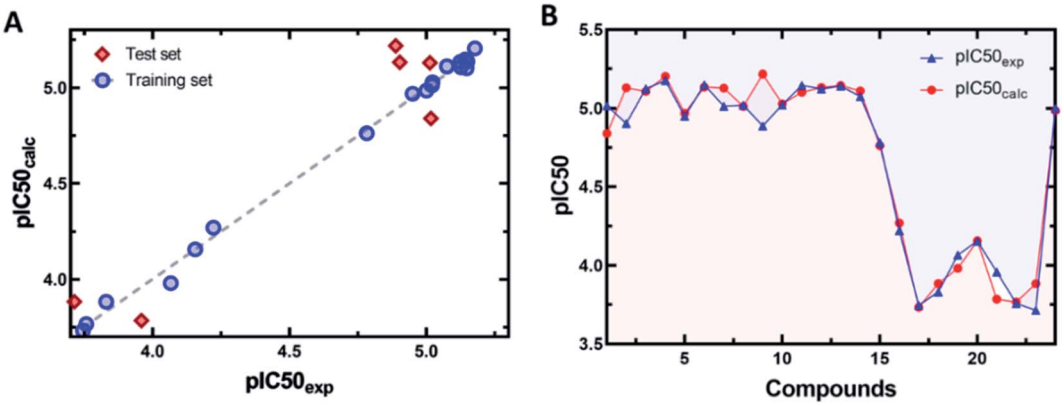

Fig. 6 (A) Scatter plots of predicted *versus* experimental activity. (B) Residual plots between predicted and experimental values.

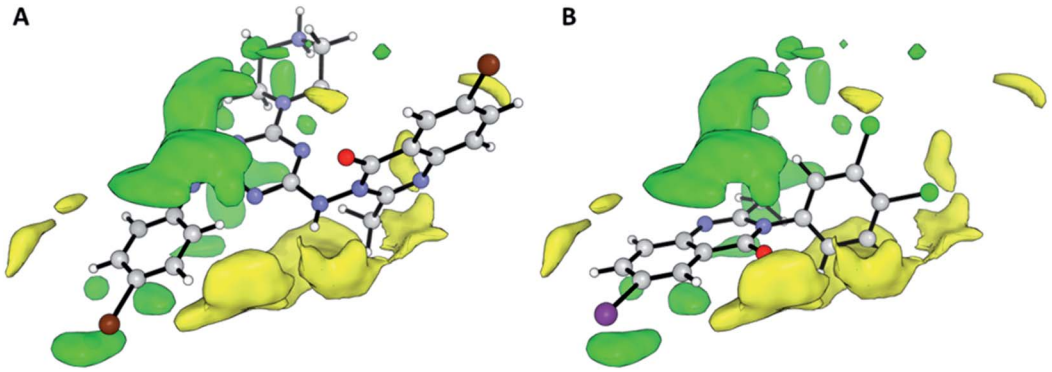

Fig. 7 Steric contour maps representing the COMFA model for cytotoxic activity. The compounds shown are the strongest (A; Pakhar_3) and weakest (B; 3d). Green and yellow regions indicate areas where steric interactions increase and decrease activity, respectively.

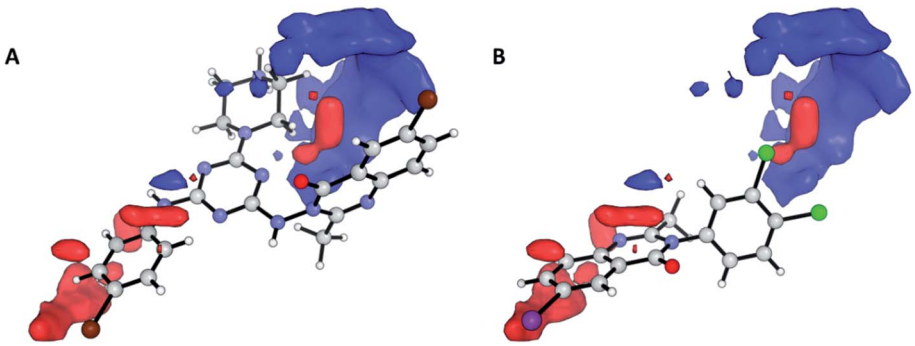

Fig. 8 Electrostatic contour maps representing the COMFA model for cytotoxic activity. Compounds shown are the strongest (A; 3) and weakest (B; 17). Blue and red regions denote enhancing and detrimental electrostatic effects with the positively charged probe, respectively.

Table 4 Prediction of the lipophilicity of the synthesized compounds

Comp.	iLOGP[39]	XLOGP3 (ref. 40)	MLOGP[41]	Consensus log *P*
3a	3.28	3.48	4.26	3.95
3b	3.17	3.41	4.15	3.86
3c	3.20	2.76	3.30	3.31
3d	3.30	4.34	4.65	4.43
3e	3.42	3.68	3.80	3.90
3f	3.36	3.03	2.97	3.34
3g	2.53	2.61	2.63	2.55
3h	3.16	3.81	4.53	4.21
3i	2.60	3.40	3.87	3.25
3j	2.61	2.61	2.63	2.57
3k	3.36	3.81	4.38	4.09
3l	3.02	3.61	3.83	3.95
3m	2.52	2.43	3.06	2.90
3n	2.86	3.54	3.13	3.16

3e (second slightly active compound) does comply with all five drug-likeness rules.

3 Experimental

3.1 Synthesis

Melting points were determined on a Kofler-type apparatus and were uncorrected. The IR spectra were taken on a PerkinElmer 200 spectrophotometer with KBr. NMR spectra were collected in DMSO-d_6 or CD_3OD with a Varian Unity Inova 500 MHz spectrometer. Chemical shifts were reported in parts per million (δ) using the residual solvent signals (DMSO-d_6: δ_H 2.50, δ_C 39.5 or CD_3OD; δ_H H 3.31, δ_C C 49.0) as the internal standards for the ^1H and ^{13}C NMR-APT spectra and coupling constants (J) in Hz. HRMS spectra were recorded on a Micromass-LCT Premier Time-of-Flight ESI spectrometer with an acquity ultra-high-performance liquid chromatography interface system. TLC was performed on Si gel Merck 60 F_{254} (Al plates) and the TLC plates were visualized by spraying with phosphomolybdic acid reagent and heating. The starting materials and reagents were purchased from Sigma–Aldrich or Merck.

3.1.1 Synthesis of 5-iodoanthranilic acid (1). Iodine (7.36 g, 29.0 mmol) was added to a solution of anthranilic acid (8.0 g, 58.3 mmol) in ethanol (112 mL) was stirred at room temperature for 5 min. Then, the reaction was heated to 80 °C and a solution of H_2O_2 (30 wt% in H_2O, 16 mL) was added dropwise for 30 min. After stirring the mixture for another 30 min at this temperature, a solution of $Na_2S_2O_5$ (10%, 136 mL) was added. Finally, H_2O (640 mL) was added, forming a precipitate which was filtered under vacuum. The residue was dried at 102 °C for 2 h. The resulting solid was recrystallized from EtOH to obtain 13.47 g (88% yield) of acid **1** as brown crystals. R_f: 0.63 (benzene/acetone/methanol/acetic acid 60 : 32 : 7.6 : 0.4). mp. 228–

Table 5 Prediction of the water solubility of the synthesized compounds[a]

	ESOL[42]		Ali[43]	
Comp.	log *S*	Class	log *S*	Class
3a	−5.29	Mod. soluble	−3.90	Soluble
3b	−4.97	Mod. soluble	−3.82	Soluble
3c	−4.44	Mod. soluble	−3.34	Soluble
3d	−5.74	Mod. soluble	−4.79	Mod. soluble
3e	−5.21	Mod. soluble	−4.30	Mod. soluble
3f	−4.68	Mod. soluble	−3.82	Soluble
3g	−4.41	Mod. soluble	−3.95	Soluble
3h	−5.31	Mod. soluble	−4.24	Mod. soluble
3i	−4.78	Mod. soluble	−4.06	Mod. soluble
3j	−4.41	Mod. soluble	−3.95	Soluble
3k	−5.16	Mod. soluble	−4.24	Mod. soluble
3l	−5.16	Mod. soluble	−4.36	Mod. soluble
3m	−4.24	Mod. soluble	−3.23	Soluble
3n	−5.19	Mod. soluble	−4.92	Mod. soluble

[a] Mod. soluble = Moderately soluble.

Table 6 Drug likeness of synthesized molecules based on Lipinski, Ghose, Veber, Egan, and Muegge rules

Comp.	Lipinski	Ghose	Veber	Egan	Muegge
3a	No	Yes	Yes	Yes	Yes
3b	Yes	Yes	Yes	Yes	Yes
3c	Yes	Yes	Yes	Yes	Yes
3d	No	Yes	Yes	Yes	Yes
3e	Yes	Yes	Yes	Yes	Yes
3f	Yes	Yes	Yes	Yes	Yes
3g	Yes	Yes	Yes	Yes	Yes
3h	No	Yes	Yes	Yes	Yes
3i	Yes	Yes	Yes	Yes	Yes
3j	Yes	Yes	Yes	Yes	Yes
3k	No	Yes	Yes	Yes	Yes
3l	Yes	Yes	Yes	Yes	Yes
3m	Yes	Yes	Yes	Yes	Yes
3n	Yes	Yes	Yes	Yes	Yes

230 °C. IR (cm^{-1}) *ν*: 3501, 3388 (N–H); 2919, 2623 (O–H); 1677 (C=O); 1613 (C_{Ar}–NH_2); 1579 (C_{Ar}–C_{Ar}); 1228 (C_{sp2}–OH). ^{1}H NMR (500 MHz, CD_3OD) *δ* (ppm): 8.05 (s, 1H), 7.43 (d, *J* = 8.73 Hz, 1H), 6.56 (d, *J* = 8.76 Hz, 1H). ^{13}C NMR-APT (126 MHz, CD_3OD) *δ* (ppm): 169.9 (CO), 147.9 (C), 141.6 (CH), 139.2 (CH), 120.7 (CH), 112.2 (C), 79.5 (C). HRMS-ESI calculated for $C_7H_7INO_2$ $[M + H]^+$: 263.99215, found 263.95447.

3.1.2 Synthesis of 2-acetamido-5-iodobenzoic acid (2). A mixture of 5-iodo anthranilic acid (**1**) (4.0 g, 15.2 mmol) and acetic anhydride (6.24 mL, 66.14 mmol) was stirred at room temperature for 5 min and then was warmed to reflux for 15 min. After cooling, distilled water (4.0 mL) was added and the solution was warmed to reflux for 2 h. The crude solution was stirred at room temperature for 24 h and the resulting precipitate was filtered and washed with small amounts of cold methanol. The resulting solid was crystallized from ethanol, to give 3.44 g (75% yield) of **2** as light brown crystals. R_f: 0.5 (benzene/acetone/methanol/acetic acid 60 : 32 : 7.6 : 0.4). mp. 239–241 °C. IR (cm^{-1}) *ν*: 3235 (N–H); 3120 (C_{Ar}–H); 2923, 2866, 2763 (O–H); 1687, 1650 (C=O); 1592 (C_{Ar}–NH_2); 1572 (C_{Ar}–C_{Ar}). ^{1}H NMR (500 MHz, DMSO-d_6) *δ* (ppm): 10.94 (s, 1H), 8.25 (d, *J* = 8.84, 1H), 8.18 (s, 1H), 7.84 (d, *J* = 8.83 Hz, 1H), 2.12 (s, 3H). ^{13}C NMR-APT (126 MHz, DMSO-d_6) *δ* (ppm): 168.5 (CO), 168.1 (CO), 142.1 (CH), 140.4 (C), 138.9 (CH), 122.1 (CH), 118.6 (C), 85.5 (C), 25.0 (CH_3). HRMS-ESI Calculated for $C_9H_9INO_3$ $[M + H]^+$: 305.96271, found 305.96454.

3.1.3 General procedure for the synthesis of 6-iodo-2-methylquinazolin-4(3*H*)-one derivatives (3a–n). A solution of PCl_3 (0.35 mL, 4.01 mmol) in dry toluene (15 mL) was slowly added (15 min) to a solution of 5-iodo-*N*-acetyl anthranilic acid (**2**) (2.0 g, 6.56 mmol) and the corresponding amine (R-NH_2) (7.26 mmol) in dry toluene (135 mL) at room temperature. The resulting mixture was warmed to reflux (110 °C) for 6 to 48 h (until the reaction was completed which was confirmed by TLC, see times in Scheme 2). Then, the mixture was allowed to cool to room temperature and was neutralized with Na_2CO_3 (sat.) followed by extraction with chloroform (4 × 100 mL). The organic phase was washed with H_2O (3 × 100 mL), dried over Na_2SO_4, filtered and concentrated under vacuum. The products were purified by crystallization with MeOH or purified by column chromatography (SiO_2, 20–50% AcOEt/hexanes).

*3.1.3.1 6-Iodo-2-methyl-3-(4-bromophenyl)-4-(3H)-quinazolinone (**3a**).* R_f: 0.83 (benzene/acetone/methanol/acetic acid 60 : 32 : 7.6 : 0.4). IR (cm^{-1}) *ν*: 3066 (C_{Ar}–H); 2925 (C_{sp3}–H); 1685 (C=O); 1598 (C=N); 1575 (C_{Ar}–C_{Ar}). ^{1}H NMR (500 MHz, DMSO-d_6) *δ* (ppm): 8.34 (s, 1H), 8.11 (d, *J* = 8.54 Hz, 1H), 7.77 (d, *J* = 8.58, 2H), 7.45 (d, *J* = 8.59 Hz, 2H), 7.43 (d, *J* = 8.65 Hz, 1H), 2.12 (s, 3H). ^{13}C NMR-APT (126 MHz, DMSO-d_6) *δ* (ppm): 159.9 (CO), 154.9 (C), 146.5 (C), 142.9 (CH), 136.9 (C), 134.4 (CH), 132.6 (2 CH), 130.7 (2 CH), 128.9 (C), 122.3 (CH), 122.2 (C), 91.1 (C–I), 24.1 (CH_3). HRMS-ESI calculated for $C_{15}H_{11}BrIN_2O$ $[M + H]^+$: 440.90994, found 440.91055.

*3.1.3.2 6-Iodo-2-methyl-3-(4-chlorophenyl)-4-(3H)-quinazolinone (**3b**).* R_f: 0.80 (benzene/acetone/methanol/acetic acid 60 : 32 : 7.6 : 0.4). IR (cm^{-1}) *ν*: 3086, 3058, 3034 and 3007 (C_{Ar}–H); 2930 (C_{sp3}–H); 1676 (C=O); 1604 (C=N); 1587 (C_{Ar}–C_{Ar}). ^{1}H NMR (500 MHz, DMSO-d_6) *δ* (ppm): 8.33 (s, 1H), 8.10 (d, *J* = 8.54 Hz, 1H), 7.64 (d, *J* = 8.74 Hz, 2H), 7.51 (d, *J* = 8.77 Hz, 2H), 7.44 (d, *J* = 8.55 Hz, 1H), 2.12 (s, 3H). ^{13}C NMR-APT (126 MHz, DMSO-d_6) *δ* (ppm): 159.9 (CO), 154.9 (C), 146.5 (C), 142.9 (CH), 136.4 (CH), 134.4 (C), 133.7 (C), 130.3 (2 C), 129.6 (2 C), 128.8 (CH), 122.2 (C), 91.1 (C–I), 24.1 (CH_3). HRMS-ESI calculated for $C_{15}H_{11}ClIN_2O$ $[M + H]^+$: 396.96046, found 396.96112.

*3.1.3.3 6-Iodo-2-methyl-3-(4-methoxiphenyl)-4-(3H)-quinazolinone (**3c**).* R_f: 0.83 (benzene/acetone/methanol/acetic acid 60 : 32 : 7.6 : 0.4). IR (cm^{-1}) *ν*: 3081, 3052 and 3003 (C_{Ar}–H); 2960 and 2934 (C_{sp3}–H); 1672 (C=O); 1610 (C=N); 1598 (C_{Ar}–C_{Ar}); 1246, 1027 (C–O). ^{1}H NMR (500 MHz, DMSO-d_6) *δ* (ppm): 8.36 (s, 1H), 8.11 (d, *J* = 8.54 Hz, 1H), 7.45 (d, *J* = 8.55 Hz, 1H), 7.34 (d, *J* = 8.84 Hz, 2H), 7.09 (d, *J* = 8.88 Hz, 2H), 3.83 (s, 3H), 2.12 (s, 3H). ^{13}C NMR-APT (126 MHz, DMSO-d_6) *δ* (ppm): 160.2 (CO), 159.3 (C), 155.9 (C), 146.6 (C), 142.8 (CH), 134.5 (CH), 130.1 (C), 129.4 (2 C), 128.9 (CH), 122.4 (C), 114.7 (2 C), 90.9 (CI), 55.4 (CH_3), 24.1 (CH_3). HRMS-ESI calculated for $C_{16}H_{14}IN_2O_2$ $[M + H]^+$: 393.00999, found 393.01059.

*3.1.3.4 6-Iodo-2-methyl-3-(3,4-dichlorophenyl)-4-(3H)-quinazolinone (**3d**).* R_f: 0.85 (benzene/acetone/methanol/acetic acid 60 : 32 : 7.6 : 0.4). IR (cm^{-1}) ν: 3061 (C_{Ar}–H); 2928 (C_{sp3}–H); 1671 (C=O); 1603 (C=N); 1587 (C_{Ar}–C_{Ar}). ^{1}H NMR (500 MHz, DMSO-d_6) δ (ppm): 8.35 (d, J = 2.0 Hz, 1H), 8.13 (dd, J = 8.5, 2.0 Hz, 1H), 7.91 (d, J = 2.3 Hz, 1H), 7.86 (d, J = 8.5 Hz, 1H), 7.54 (dd, J = 8.5, 2.3 Hz, 1H), 7.46 (d, J = 8.5 Hz, 1H),2.15 (s, 3H). ^{13}C NMR-APT (126 MHz, DMSO-d_6) δ (ppm): 159.9 (CO), 154.7 (C), 146.5 (C), 143.0 (CH), 137.4 (C), 134.4 (CH), 132.1 (CH), 131.9 (C), 131.5 (C), 130.8 (CH), 129.1 (CH), 128.9 (CH), 122.2 (C), 91.2 (C–I), 24.0 (CH_3). HRMS-ESI calculated for $C_{15}H_{10}Cl_2IN_2O$ $[M + H]^+$: 430.92148, found 430.91843.

*3.1.3.5 6-Iodo-2-methyl-3-(3-chloro-4-methoxiphenyl)-4-(3H)-quinazolinone (**3e**).* R_f: 0.78 (benzene/acetone/methanol/acetic acid 60 : 32 : 7.6 : 0.4). IR (cm^{-1}) ν: 3062, 3006 (C_{Ar}–H); 2965, 2942, 2927 (C_{sp3}–H); 1675 (C=O); 1609 (C=N); 1592 (C_{Ar}–C_{Ar}); 1264, 1058 (C–O). ^{1}H NMR (500 MHz, DMSO-d_6) δ (ppm): 8.35 (d, J = 2.0 Hz, 1H), 8.12 (dd, J = 8.5, 2.1 Hz, 1H), 7.63 (d, J = 2.5 Hz, 1H), 7.45 (d, J = 8.6 Hz, 1H), 7.42 (dd, J = 8.7, 2.5 Hz, 1H), 7.31 (d, J = 8.8 Hz, 1H), 3.94 (s, 3H), 2.14 (s, 3H). ^{13}C NMR-APT (126 MHz, DMSO-d_6) δ (ppm): 160.2 (CO), 155.5 (C), 154.9 (C), 146.6 (C), 142.9 (CH), 134.5 (CH), 130.4 (C), 129.7 (CH), 128.9 (CH), 128.4 (CH), 122.3 (C), 121.3 (C), 113.2 (CH), 91.0 (C–I), 56.4 (CH_3), 24.1 (CH_3). HRMS-ESI calculated for $C_{16}H_{13}ClIN_2O_2$ $[M + H]^+$: 426.97102, found 426.97101.

*3.1.3.6 6-Iodo-2-methyl-3-(3,4-dimethoxiphenyl)-4-(3H)-quinazolinone (**3f**).* R_f: 0.80 (benzene/acetone/methanol/acetic acid 60 : 32 : 7.6 : 0.4). IR (cm^{-1}) ν: 3062 (C_{Ar}–H); 2997, 2962, 2962, 2934 (C_{sp3}–H); 1673 (C=O); 1608 (C=N); 1590 (C_{Ar}–C_{Ar}); 1249, 1132 (C–O). ^{1}H NMR (500 MHz, DMSO-d_6) δ (ppm): 8.36 (d, J = 2.0 Hz, 1H), 8.11 (dd, J = 8.5, 2.1 Hz, 1H), 7.44 (d, J = 8.6 Hz, 1H), 7.11–7.07 (m, 2H), 6.95 (dd, J = 8.4, 2.4 Hz, 1H),3.83 (s, 3H), 3.74 (s, 3H), 2.16 (s, 3H). ^{13}C NMR-APT (126 MHz, DMSO-d_6) δ (ppm): 160.1 (CO), 155.9 (C), 149.3 (C), 148.9 (C), 146.6 (C), 142.7 (CH), 134.5 (CH), 130.2 (CH), 128.8 (CH), 122.4 (CH), 120.2 (C), 111.9 (CH), 111.8 (CH), 90.9 (C–I), 55.7 (CH_3), 55.6 (CH_3), 23.9 (CH_3). HRMS-ESI calculated for $C_{17}H_{16}IN_2O_3$ $[M + H]^+$: 423.02056, found 423.01840.

*3.1.3.7 6-Iodo-2-methyl-3-(4-nitrophenyl)-4-(3H)-quinazolinone (**3g**).* R_f: 0.85 (benzene/acetone/methanol/acetic acid 60 : 32 : 7.6 : 0.4). IR (cm^{-1}) ν: 3112, 3071 (C_{Ar}–H); 2976, 2930 (C_{sp3}–H); 1679 (C=O); 1602 (C=N); 1579 (C_{Ar}–C_{Ar}); 1520 (C–NO_2); 1354 (C–NO_2). ^{1}H NMR (500 MHz, DMSO-d_6) δ (ppm): 8.42 (d, J = 9.0 Hz, 2H), 8.37 (d, J = 2.0 Hz, 1H), 8.15 (dd, J = 8.5, 2.1 Hz, 1H), 7.82 (d, J = 9.0 Hz, 2H), 7.48 (d, J = 8.6 Hz, 1H),2.13 (s, 3H). ^{13}C NMR-APT (126 MHz, DMSO-d_6) δ (ppm): 159.9 (CO), 154.3 (C), 147.7 (C), 146.6 (C), 143.3 (CH), 143.1 (C), 134.4 (CH), 130.3 (2 CH), 128.9 (CH), 124.8 (2 CH), 122.2 (C), 91.3 (C–I), 24.0 (CH_3). HRMS-ESI calculated for $C_{15}H_{11}IN_3O_3$ $[M + H]^+$: 407.98450, found 407.98343.

*3.1.3.8 6-Iodo-2-methyl-3-(3-chloro-4-fluorophenyl)-4-(3H)-quinazolinone (**3h**).* R_f: 0.82 (benzene/acetone/methanol/acetic acid 60 : 32 : 7.6 : 0.4). IR (cm^{-1}) ν: 3063 (C_{Ar}–H); 2926 (C_{sp3}–H); 1671 (C=O); 1603 (C=N); 1558 (C_{Ar}–C_{Ar}).^{1}H NMR (500 MHz, DMSO-d_6) δ (ppm): 8.36 (d, J = 2.0 Hz, 1H), 8.13 (dd, J = 8.5, 2.1 Hz, 1H), 7.87 (dd, J = 6.7, 2.5 Hz, 1H), 7.64 (t, J = 9.0 Hz, 1H), 7.58–7.52 (m, 1H), 7.46 (d, J = 8.5 Hz, 1H), 2.14 (s, 3H). ^{13}C NMR-APT (DMSO-d_6, 126 MHz) δ (ppm): 160.0 (CO), 157.3 (d, J = 248.9 Hz, C), 154.9 (C), 146.5 (C), 143.0 (CH), 134.5 (CH), 134.4 (C), 130.9 (CH), 129.6 (d, J = 8.0 Hz, CH), 128.9 (CH), 122.2 (C), 120.2 (d, J = 18.8 Hz, C), 117.8 (d, J = 22.1 Hz, CH), 91.1 (C–I), 24.1 (CH_3). HRMS-ESI calculated for $C_{15}H_{10}ClFIN_2O$ $[M + H]^+$: 414.95103, found 414.95044.

*3.1.3.9 6-Iodo-2-methyl-3-(1-phenylamino)-4-(3H)-quinazolinone (**3i**).* R_f: 0.80 (benzene/acetone/methanol/acetic acid 60 : 32 : 7.6 : 0.4). IR (cm^{-1}) ν: 3239 (N–H); 3066, 3021 (C_{Ar}–H); 2964, 2929 (C_{sp3}–H); 1672 (C=O); 1600 (C=N); 1588 (C_{Ar}–C_{Ar}). ^{1}H NMR (500 MHz, DMSO-d_6) δ (ppm): 9.12 (s, 1H), 8.33 (d, J = 2.0 Hz, 1H), 8.12 (dd, J = 8.6, 2.1 Hz, 1H), 7.47 (d, J = 8.6 Hz, 1H), 7.19 (dd, J = 8.4, 7.5 Hz, 2H), 6.85 (t, J = 7.3 Hz, 1H), 6.66 (d, J = 7.7 Hz, 2H), 2.49 (s, 3H). ^{13}C NMR-APT (126 MHz, DMSO-d_6) δ (ppm): 158.9 (CO), 158.5 (C), 146.5 (C), 146.0 (C), 143.0 (CH), 134.3 (CH), 129.2 (2 CH), 129.1 (CH), 122.9 (CH), 120.4 (C), 112.4 (2 CH), 91.3 (C–I), 21.5 (CH_3). HRMS-ESI calculated for $C_{15}H_{13}IN_3O$ $[M + H]^+$: 378.01032, found 378.01184.

*3.1.3.10 6-Iodo-2-methyl-3-(3-nitrophenyl)-4-(3H)-quinazolinone (**3j**).* R_f: 0.85 (benzene/acetone/methanol/acetic acid 60 : 32 : 7.6 : 0.4). IR (cm^{-1}) ν: 3073 (C_{Ar}–H); 2932 (C_{sp3}–H); 1673 (C=O); 1616 (C=N); 1599 (C_{Ar}–C_{Ar}); 1531, 1349 (NO_2). ^{1}H NMR (500 MHz, DMSO-d_6) δ (ppm): 8.49 (t, J = 2.0 Hz, 1H), 8.41–8.37 (m, 1H), 8.36 (d, J = 1.5 Hz, 1H), 8.14 (dt, J = 8.5, 1.7 Hz, 1H), 8.01–7.95 (m, 1H), 7.88 (t, J = 8.1 Hz, 1H), 7.47 (dd, J = 8.5, 0.8 Hz, 1H), 2.13 (s, 3H). ^{13}C NMR-APT (126 MHz, DMSO-d_6) δ (ppm): 160.1 (CO), 154.6 (C), 148.5 (C), 146.6 (C), 143.0 (CH), 138.6 (C), 135.4 (CH), 134.4 (CH), 130.9 (CH), 128.9 (CH), 124.1 (2 CH), 122.3 (C), 91.2 (C–I), 24.1 (CH_3). HRMS-ESI calculated for $C_{15}H_{11}IN_3O_3$ $[M + H]^+$: 407.98450, found 407.98532.

*3.1.3.11 6-Iodo-2-methyl-3-(3,4-dimethylphenyl)-4-(3H)-quinazolinone (**3k**).* R_f: 0.83 (benzene/acetone/methanol/acetic acid 60 : 32 : 7.6 : 0.4). IR (cm^{-1}) ν: 3048, 3019 (C_{Ar}–H); 2972, 2915 (C_{sp3}–H); 1667 (C=O); 1596 (C=N); 1576 (C_{Ar}–C_{Ar}). ^{1}H NMR (500 MHz, DMSO-d_6) δ (ppm): 8.34 (d, J = 2.0 Hz, 1H), 8.10 (dd, J = 8.5, 2.1 Hz, 1H), 7.44 (d, J = 8.6 Hz, 1H), 7.31 (d, J = 8.0 Hz, 1H), 7.18 (s, 1H), 7.12 (dd, J = 7.9, 2.0 Hz, 1H), 2.30 (s, 3H), 2.27 (s, 3H), 2.12 (s, 3H). ^{13}C NMR-APT (126 MHz, DMSO-d_6) δ (ppm): 160.0 (CO), 155.5 (C), 146.6 (C), 142.8 (CH), 137.7 (C), 137.3 (CH), 135.1 (C), 134.4 (C), 130.4 (CH), 128.8 (CH), 128.8 (CH), 125.3 (CH), 122.3 (C), 90.9 (C–I), 24.1 (CH_3), 19.3 (CH_3), 19.0 (CH_3). HRMS-ESI calculated for $C_{17}H_{16}IN_2O$ $[M + H]^+$: 391.03073, found 391.03262.

*3.1.3.12 6-Iodo-2-methyl-3-[-2-(3-indolyl)-ethyl]-4-(3H)-quinazolinone (**3l**).* Purified by column chromatography. R_f: 0.78 (benzene/acetone/methanol/acetic acid 60 : 32 : 7.6 : 0.4). IR (cm^{-1}) ν: 3329 (N–H); 3062, 3010 (C_{Ar}–H); 2979, 2917 (C_{sp3}–H); 1656 (C=O); 1616 (C=N); 1589 (C_{Ar}–C_{Ar}). ^{1}H NMR (500 MHz, DMSO-d_6) δ (ppm): 10.90 (s, 1H), 8.43 (d, J = 2.1 Hz, 1H), 8.07 (dd, J = 8.5, 2.1 Hz, 1H), 7.62 (d, J = 7.8 Hz, 1H), 7.36 (dd, J = 8.3, 5.8 Hz, 2H), 7.18 (d, J = 2.3 Hz, 1H), 7.08 (ddd, J = 8.1, 6.9, 1.2 Hz, 1H), 6.98 (ddd, J = 8.0, 6.9, 1.1 Hz, 1H), 4.30–4.23 (m, 2H), 3.12–3.05 (m, 2H), 2.45 (s, 3H). ^{13}C NMR-APT (126 MHz, DMSO-d_6) (ppm): 159.88 (CO), 155.86 (C), 146.36 (C), 142.58 (CH), 136.22 (CH), 134.44 (C), 128.79 (C), 127.07 (CH), 123.34 (CH), 121.91 (CH), 121.14 (C), 118.50 (CH), 118.15 (CH), 111.52

(C), 110.47 (CH), 90.98 (C–I), 45.33 (CH_2), 23.53 (CH_2), 22.81 (CH_3). HRMS-ESI calculated for $C_{19}H_{17}IN_3O$ $[M + H]^+$: 430.04162, found 430.03720.

*3.1.3.13 6-Iodo-2-methyl-3-(4-hydroxyphenyl)-4-(3H)-quinazolinone (**3m**).* Purified by column chromatography. R_f: 0.85 (benzene/acetone/methanol/acetic acid 60 : 32 : 7.6 : 0.4). IR (cm^{-1}) ν: 3202 (O–H); 3081, 3033 (C_{Ar}–H); 2935 (C_{sp3}–H); 1652 (C=O); 1613 (C=N); 1598 (C_{Ar}–C_{Ar}); 1270 (C–O). ^{1}H NMR (500 MHz, DMSO-d_6) δ (ppm): 9.85 (s, 1H), 8.33 (d, J = 2.1 Hz, 1H), 8.09 (dd, J = 8.5, 2.1 Hz, 1H), 7.43 (d, J = 8.5 Hz, 1H), 7.19 (d, J = 8.7 Hz, 2H), 6.89 (d, J = 8.7 Hz, 2H), 2.11 (s, 3H). ^{13}C NMR-APT (126 MHz, DMSO-d_6) δ (ppm): 160.3 (CO), 157.7 (C), 156.1 (C), 146.6 (C), 142.8 (CH), 134.5 (CH), 129.2 (C), 128.9 (2 CH), 128.6 (CH), 122.4 (C), 116.0 (2 CH), 91.0 (C–I), 24.2 (CH_3). HRMS-ESI calculated for $C_{15}H_{12}IN_2O_2$ $[M + H]^+$: 378.99434, found 378.99564.

*3.1.3.14 6-Iodo-2-methyl-3-(4-chloro2-nitrophenyl)-4-(3H)-quinazolinone (**3n**).* Purified by column chromatography. R_f: 0.88 (benzene/acetone/methanol/acetic acid 60 : 32 : 7.6 : 0.4). IR (cm^{-1}) ν: 3212, 3082, 3018 (C_{Ar}–H); 2967, 2923 (C_{sp3}–H); 1681 (C=O); 1603 (C=N); 1592 (C_{Ar}–C_{Ar}); 1527, 1348 (C–NO_2). ^{1}H NMR (500 MHz, DMSO-d_6) δ (ppm): 8.44 (d, J = 2.4 Hz, 1H), 8.34 (d, J = 2.0 Hz, 1H), 8.18 (dd, J = 8.5, 2.1 Hz, 1H), 8.12 (m, 1H), 7.94 (d, J = 8.5 Hz, 1H), 7.50 (d, J = 8.6 Hz, 1H), 2.23 (s, 3H). ^{13}C NMR-APT (126 MHz, DMSO-d_6) δ (ppm): 159.6 (CO), 154.3 (C), 146.4 (C), 146.0 (CH), 143.6 (C), 135.4 (C), 135.2 (CH), 134.4 (CH), 133.0 (CH), 129.2 (C), 129.0 (CH), 126.0 (CH), 121.4 (C), 91.8 (C–I), 23.7 (CH_3). HRMS-ESI calculated for $C_{15}H_{10}ClIN_3O_3$ $[M + H]^+$: 441.94553, found 441.94547.

3.2 Cytotoxicity assay

Human gallbladder adenocarcinoma (G415), human gallbladder adenocarcinoma (Gbd1), human promyelocytic leukemia (HL60), human histiocytic lymphoma (U937), human cervix adenocarcinoma (HeLa) and human brain glioblastoma multiforma (T98G) cell lines were purchased from the American Type Culture Collection (Manassas, VA, USA). All cell lines were grown at 37 °C in a humidified atmosphere of 5% CO_2 environment and the adherent cells were removed from culture plates by trypsinization (0.5 mM EDTA, 0.05% trypsin). G-415 and Gbd1 were maintained in RPMI 1640 supplemented with 2 mM glutamine, 10% FBS, penicillin/streptomycin/amphotericin-B (100 units per mL; 100 μg mL^{-1}; 0.25 μg mL^{-1}). Confluent cultures of these two adherent cell lines were split 1 : 3 to 1 : 6 by trypsinization and seeded at 2–4 × 10^4 cells per cm^2. HL60 and U937 cells were grown in the same medium and seeded at 1–5 × 10^5 and 2–9 × 10^5 cells per mL, respectively. Three times per week, the culture cells were diluted under the same conditions to maintain density and were harvested in the exponential phase of growth. HeLa cells were cultured in MEM, containing 2 mM glutamine, 10% FBS, 1% non-essential amino acids, penicillin/streptomycin/amphotericin-B (100 units per mL; 100 μg mL^{-1}; 0.25 μg mL^{-1}). T98G cells were grown in DMEM-F12 supplemented with 2 mM glutamine, 10% FBS, 1% non-essential amino acids, 1% sodium pyruvate, penicillin/streptomycin/amphotericin-B (100 units per mL; 100 μg mL^{-1}; 0.25 μg mL^{-1}). Confluent cultures of these last two adherent cell lines were split 1 : 3 to 1 : 6 by trypsinization and seeded at 2–4 × 10^4 cells per cm^2. For cytotoxicity studies, cells were seeded in a 96-well microtiter plate at a density of 5 × 10^5 mL^{-1} and allowed to adhere for 24 h in a CO_2 incubator. One day after seeding, cells were treated with fresh medium containing the compounds, dissolved in DMSO (1% final concentration in the well) plus culture medium, incubating by 24 h at 37 °C. The compound concentrations ranged from 0 μM up to 200 μM. After incubation, 10 μL aliquots of MTT solution (5 mg mL^{-1} in PBS) were added to each well and re-incubated for 4 h at 37 °C, followed by low centrifugation at 800 rpm for 5 minutes. Cell viability was determined by means of MTT reduction and the cells incubated in culture medium alone and 1% DMSO served as control for cell viability (untreated cells). 200 μL of supernatant was carefully aspirated and 200 μL aliquots of 100% DMSO were added to each well to dissolve the formazan crystals, followed by incubation of 10 minutes at 37 °C to dissolve air bubbles. The culture plate was placed on an Emax model micro-plate reader (Molecular Devices) and the absorbance was measured spectrophotometrically at 650 nm. The amount of color produced is directly proportional to the number of viable cells. Untreated cells and the controls containing 1% DMSO were used as 100% viability controls (negative controls, see ESI†). Paclitaxel (T7191, Sigma-Aldrich) was used as reference compound (positive controls, see ESI†). All assays were performed twice with three replicates and processed independently. Mean ± SD was used to estimate the cell viability. Cell viability rate was calculated as the percentage of MTT absorption as follows:

$$\%\ \text{survival} = (\text{mean experimental absorbance/mean control absorbance}) \times 100$$

The compound concentration was plotted against the corresponding percentage (%) of cell viability obtained with MTT assays, and the 50% inhibitory concentration (IC_{50}) was calculated by non-linear regression. The curve fittings were performed using GraphPad Prism®6 from Systat Software, Inc. Compounds with IC_{50} > 200 μM were considered as inactive.

3.2.1 Statistical analysis. Data were compared by one-way analysis of variance Student's *t*-test to determine statistical significance (GraphPad Prism®6). Each experiment as performed in triplicate on two occasions. Results are expressed.

3.3 Computational method

The preparations of iodinated 4-(3*H*)-quinazolinone 3D structures were obtained with OpenBabel[44] from SMILES annotations for each ligand. Protonation states were adjusted to pH 7.2 using FixpKa and AM1BCC charges implemented in the QUACPAC package,[45] followed by conformer generation using OMEGA.[46] Docking was performed using FRED[47] and the coordinates of the co-crystal structure of DFHR (PDB code 4M6J),[36] keeping 20 poses for each docked molecule. Optimization of the docked poses was carried out using a two-step protocol and SZYBKI.[48] First, optimization of the ligand's Cartesian coordinates was performed

using a constraint of 1 kcal mol^{-1}, followed by optimization of the complex using MMFF94 s as a force field, a Poisson–Boltzmann model, and AM1BCC charges for the ligands. Flexibility of residue side chains were kept within 6 Å of the ligand. The resulting poses were ranked according to the predicted ligand-protein energy, and the pose with the lowest score was selected as the best pose for each molecule.

3D-QSAR models were obtained with the Open3DQSAR package,[49] which performs partial least squares (PLS) regression models from molecular interaction fields (MIF). Unless otherwise noted, default parameters were employed for Open3-DQSAR. The input to Open3DQSAR is a set of aligned conformers of the dataset with associated bioactivities. A grid was constructed around the aligned molecules in such a way that its box exceeded 5 Å in the largest molecule, and grid spacing was set to 0.5 Å. Steric and electrostatic molecular mechanics of MIFs were computed using the Merck force field (MMFF94). The pictures were obtained with Chimera UCSF and PyMol software.

The prediction of drug likeness of synthesized molecules is estimated using parameters based on Lipinski, Ghose, Veber, Egan, and Muegge rules and, their lipid and water solubility by applying the SwissADME web tool (**https://www.swissadme.ch**, accessed on 5 July 2022).[50] The SwissADME synthetic accessibility score is mainly based on the assumption of the molecular.

4 Conclusions

A novel series of iodinated 4-(3*H*)-quinazolinones 3*N*-substituted were synthesized and screened for their *in vitro* cytotoxic activity against six cancer cell lines (G415, Gbd1, T98G, HeLa, HL60, and U937). Some of these compounds, **3e** and **3h**, showed remarkable cytotoxic activity against the T98G cell line with IC_{50} values similar or slightly lower than the control, paclitaxel (IC_{50} = 21 μM). Similarly, marked inhibitory activity was also observed for compounds **3a** and **3b** on cell line U937, with one of them showing greater efficiency than paclitaxel (IC_{50} = 41 μM). Additionally, compound **3a** showed important activity on HL60 cells (IC_{50} = 21 μM). Moreover, **3d** showed significant cytotoxic activity on HeLa cells (IC_{50} = 10 μM), on same order of magnitude as paclitaxel (IC_{50} = 6.2 μM). Therefore, the experimental study of these compounds should move towards *in vivo* studies, using animal models of glioblastoma (**3e** and **3h**), lymphoma (**3a** and **3b**), promyelocytic leukemia (**3a**), and cervical adenocarcinoma (**3d**). The cytotoxic activities of the new iodinated 4-(3*H*)-quinazolinones 3*N*-substituted were screened, and the molecular docking between compound **3d** and the active site of DHFR was performed through the FRED software. The results revealed that the molecular coupling of compound **3d** to the active site is similar to that of natural DHFR ligands, suggesting the inhibitory mechanism of compound **3d** on the catalytic activity of this enzyme. Moreover, based on the results of the 3D-QSAR calculations for the synthesized compounds, the structure activity relationship (SAR) can be summarized by the change of substituents at positions of the quinozoline rings. This change has an effect on cytotoxic activity. Docking results showed that higher lipophilic character and the presence of electron-withdrawing groups at the *para* position of phenyl ring has constructive impacts toward the development of new iodinated-quinazolinic compounds. It is known that the inhibition of DHFR by quinazolinones derivatives leads to cell death, for this reason the compounds of this chemical nature and that also show cytotoxic activity against various lineages of cancer cells would have possibilities not only as antineoplastic drugs, but also as biocides to various protozoan, fungal and microbial pathogens, in addition to their use in arthritis treatment. Therefore, studies of the effect of these quinazolinones on the catalytic activity of DHFR, as well as their ability as antiprotozoa, antifungal and antimicrobial agents are required, as well as testing the main active compounds in an *in vivo* study in animal models for the malignant neoplasms evaluated.

Conflicts of interest

There are no conflicts to declare.

Acknowledgements

VK thanks the European Union Project ChemBioFight (grant 269301). The biological studies were supported by grants awarded by the "Fondo Nacional de Desarrollo Científico y Tecnológico de Chile" (Fondecyt 1150934) and "Fondo de Financiamiento de Centros de Investigación en Áreas Prioritarias" (FONDAP 15110027). A. C.-A. thanks the OpenEye company for academic licenses. Powered@NLHPC: This research was partially supported by the supercomputing infrastructure of the NLHPC (ECM-02).

Notes and references

1 (*a*) M. F. Grundon, *Nat. Prod. Rep.*, 1984, **1**, 196–200; (*b*) D. He, M. Wang, S. Zhao, Y. Shu, H. Zeng, C. Xiao, C. Lu and Y. Liu, *Fitoterapia*, 2017, **119**, 136–149; (*c*) J. Bartroli, E. Turmo, M. Algueró, E. Boncompte, M. L. Vericat, L. Conte, J. Ramis, M. Merlos, J. García-Rafanell and J. Forn, *J. Med. Chem.*, 1998, **41**, 1869–1882; (*d*) I. Khan, S. Zaib, S. Batool, N. Abbas, Z. Ashraf, J. Iqbal and A. Saeed, *Bioorg. Med. Chem.*, 2016, **24**, 2361–2381; (*e*) I. Khan, A. Ibrar, N. Abbas and A. Saeed, *Eur. J. Med. Chem.*, 2014, **76**, 193–244; (*f*) V. Alagarsamy, K. Chitra, G. Saravanan, V. R. Solomon, M. T. Sulthana and B. Narendhar, *Eur. J. Med. Chem.*, 2018, **151**, 628–685.

2 (*a*) M. Hrast, K. Rožman, M. Jukič, D. Patin, S. Gobec and M. Sova, *Bioorg. Med. Chem. Lett.*, 2017, **27**, 3529–3533; (*b*) A. K. Nanda, S. Ganguli and R. Chakraborty, *Molecules*, 2007, **12**, 2413–2426; (*c*) R. Bouley, D. Ding, Z. Peng, M. Bastian, E. Lastochkin, W. Song, M. A. Suckow, V. A. Schroeder, W. R. Wolter, S. Mobashery and M. Chang, *J. Med. Chem.*, 2016, **59**, 5011–5021; (*d*) M. S. Mohameda, M. M. Kamel, E. M. Kassem, N. Abotaleb, S. I. AbdEl-Moez and M. F. Ahmed, *Eur. J. Med. Chem.*, 2010, **45**, 3311–3319; (*e*) S. Gatadi, J. Gour, M. Shukla, G. Kaul, S. Das, A. Dasgupta, S. Malasala, R. S. Borra, Y. V. Madhavi,

S. Chopra and S. Nanduri, *Eur. J. Med. Chem.*, 2018, **157**, 1056–1067.

3 (*a*) B. S. Kuarm, Y. T. Reddy, J. V. Madhav, P. A. Crooks and B. Rajitha, *Bioorg. Med. Chem. Lett.*, 2011, **21**, 524–527; (*b*) M. M. Ghorab, S. M. Abdel-Gawad and M. S. A. El-Gaby, *Farmaco*, 2000, **55**, 249–255; (*c*) S. N. Pandeya, D. Sriram, G. Nath and E. De Clercq, *Arzneim. Forsch.*, 2000, **50**, 55–59.

4 (*a*) S. Gatadi, J. Gour, M. Shukla, G. Kaul, A. Dasgupta, Y. V. Madhavi, S. Chopra and S. Nanduri, *Eur. J. Med. Chem.*, 2019, **175**, 287–308; (*b*) C. Couturier, C. Lair, A. Pellet, A. Upton, T. Kaneko, C. Perron, E. Cogo, J. Menegotto, A. Bauer, B. Scheiper, S. Lagrange and E. Bacqué, *Bioorg. Med. Chem. Lett.*, 2016, **26**, 5290–5299.

5 (*a*) S. Zhu, J. Wang, G. Chandrashekar, E. Smith, X. Liu and Y. Zhang, *Eur. J. Med. Chem.*, 2010, **45**, 3864–3869; (*b*) H. Kikuchi, K. Yamamoto, S. Horoiwa, S. Hirai, R. Kasahara, N. Hariguchi, M. Matsumoto and Y. Oshima, *J. Med. Chem.*, 2006, **49**, 4698–4706.

6 Y. Deng, H. Mu, H. B. Li, L. Z. Fu, D. Tang, T. Wu, S. H. Huang and C. H. Li, *Chem. Biodiversity*, 2021, **18**, e202100687.

7 (*a*) B. De Filippis, A. Ammazzalorso, M. Fantacuzzi, L. Giampietro, C. Maccallini and R. Amoroso, *ChemMedChem*, 2017, **12**, 558–570; (*b*) K. I. Ozaki, Y. Yamada, T. Oine, T. Ishizuka and Y. Iwasawa, *J. Med. Chem.*, 1985, **28**, 568–576; (*c*) A. A. M. Abdel-Aziz, L. A. Abou-Zeid, K. E. H. ElTahir, M. A. Mohamed, M. A. Abu El-Enin and A. S. El-Azab, *Bioorg. Med. Chem.*, 2016, **24**, 3818–3828.

8 (*a*) S. E. Abbas, F. M. Awadallah, N. A. Ibrahin, E. G. Said and G. M. Kamel, *Eur. J. Med. Chem.*, 2012, **53**, 141–149; (*b*) K. P. Rakesh, C. S. Shantharam and H. M. Manukumar, *Bioorg. Chem.*, 2016, **68**, 1–8.

9 (*a*) G. Marzaro, I. Castagliuolo, G. Schirato, G. Palu, M. Dalla Via, A. Chilin and P. Brun, *Eur. J. Med. Chem.*, 2016, **115**, 416–425; (*b*) X. Fang, Y. T. Chen, E. H. Sessions, S. Chowdhury, T. Vojkovsky, Y. Yin, J. R. Pocas, W. Grant, T. Schröter, L. Lin, C. Ruiz, M. D. Cameron, P. Lograsso, T. D. Bannister and Y. Feng, *Bioorg. Med. Chem. Lett.*, 2011, **21**, 1844–1848; (*c*) T. O. Mirgany, A. N. Abdalla, M. Arifuzzaman, A. F. M. Motiur Rahman and H. S. Al-Salem, *J. Enzyme Inhib. Med. Chem.*, 2021, **36**, 2055–2067.

10 (*a*) P. M. Chandrika, T. Yakaiah, A. R. R. Rao, B. Narsaiah, N. C. Reddy, V. Sridhar and J. V. Rao, *Eur. J. Med. Chem.*, 2008, **43**, 846–852; (*b*) L. Mosca, D. Rotili, I. Tempera, A. Masci, M. Fontana, R. Chiaraluce, P. Mastromarino, M. d'Erme and A. Mai, *ChemMedChem*, 2011, **6**, 606–611; (*c*) B. Marvania, P. C. Lee, R. Chaniyara, H. Dong, S. Suman, R. Kakadiya, T. C. Chou, T. C. Lee, A. Shah and T. L. Su, *Bioorg. Med. Chem.*, 2011, **19**, 1987–1998; (*d*) M. A. Mohamed, R. R. Ayyad, T. Z. Shawer, A. A. M. Abdel-Aziz and A. S. El-Azab, *Eur. J. Med. Chem.*, 2016, **112**, 106–113; (*e*) N. M. Abdel Gawad, H. H. Georgey, R. M. Youssef and N. A. El-Sayed, *Eur. J. Med. Chem.*, 2010, **45**, 6058–6067; (*f*) N. Manhas, P. Singh, C. Mocktar, M. Singh and N. Koorbanally, *Chem. Biodiversity*, 2021, **18**, e2100096; (*g*) C. J. Wang, X. Guo, R. Q. Zhai, C. Sun, G. Xiao, J. Chen, M. Y. Wei, C. L. Shao and Y. Gu, *Eur. J. Med. Chem.*, 2021, **224**, 113671; (*h*) E. R. Mohammed and G. F. Elmasry, *J. Enzyme Inhib. Med. Chem.*, 2022, **37**, 686–700.

11 (*a*) V. Bavetsias, J. H. Marriott, C. Melin, R. Kimbell, Z. S. Matusiak, F. T. Boyle and A. L. Jackman, *J. Med. Chem.*, 2000, **43**, 1910–1926; (*b*) J. B. Smaill, G. W. Rewcastle, J. A. Loo, K. D. Greis, O. H. Chan, E. L. Reyner, E. Lipka, H. D. H. Showalter, P. W. Vincent, W. L. Elliott and W. A. Denny, *J. Med. Chem.*, 2000, **43**, 1380–1397; (*c*) A. Wissner, D. M. Berger, D. H. Boschelli, M. Brawner Floyd, L. M. Greenberger, B. C. Gruber, B. D. Johnson, N. Mamuya, R. Nilakantan, M. F. Reich, R. Shen, H. R. Tsou, E. Upeslacis, Y. F. Wang, B. Wu, F. Ye and N. Zhang, *J. Med. Chem.*, 2000, **43**, 3244–3256.

12 (*a*) H. S. A. ElZahabi, M. S. Nafie, D. Osman, N. H. Elghazawy, D. H. Soliman, A. A. H. EL-Helby and R. K. Arafa, *Eur. J. Med. Chem.*, 2021, **222**, 113609; (*b*) A. M. Soliman, A. Khalil, E. Ramadan and M. M. Ghorab, *Bioorg. Med. Chem. Lett.*, 2021, **49**, 128308; (*c*) M. W. Aziz, A. M. Kamal, K. O. Mohamed and A. A. Elgendy, *Bioorg. Med. Chem. Lett.*, 2021, **41**, 127987.

13 (*a*) K. El-Adl, A. G. A. El-Helby, R. R. Ayyad, H. A. Mahdy, M. M. Khalifa, H. A. Elnagar, A. B. M. Mehany, A. M. Metwaly, M. A. Elhendawy, M. M. Radwan, M. A. ElSohly and I. H. Eissa, *Bioorg. Med. Chem.*, 2021, **29**, 115872; (*b*) H. A. Mahdy, M. K. Ibrahim, A. M. Metwaly, A. Belal, A. B. M. Mehany, K. M. A. El-Gamal, A. El-Sharkawy, M. A. Elhendawy, M. M. Radwan, M. A. Elsohly and I. H. Eissa, *Bioorg. Chem.*, 2020, **94**, 103422; (*c*) I. H. Eissa, A. G. A. El-Helby, H. A. Mahdy, M. M. Khalifa, H. A. Elnagar, A. B. M. Mehany, A. M. Metwaly, M. A. Elhendawy, M. M. Radwan, M. A. ElSohly and K. El-Adl, *Bioorg. Chem.*, 2020, **105**, 104380.

14 (*a*) M. A. Sabry, H. A. Ewida, G. S. Hassan, M. A. Ghaly and H. I. El-Subbagh, *Bioorg. Chem.*, 2019, **88**, 102923; (*b*) S. M. El-Messery, G. S. Hassan, M. N. Nagi, E. S. E. Habib, S. T. Al-Rashood and H. I. El-Subbagh, *Bioorg. Med. Chem. Lett.*, 2016, **26**, 4815–4823; (*c*) S. T. Al-Rashood, G. S. Hassan, S. M. El-Messery, M. N. Nagi, E. S. E. Habib, F. A. M. Al-Omary and H. I. El-Subbagh, *Bioorganic Med. Chem. Lett.*, 2014, **24**, 4557–4567.

15 A. Gangjee, J. Yu, J. J. McGuire, V. Cody, N. Galitsky, R. L. Kisliuk and S. F. Queener, *J. Med. Chem.*, 2000, **43**, 3837–3851.

16 J.-F. Liu, *Curr. Org. Synth.*, 2007, **4**, 223–237.

17 (*a*) H. T. B. Bui, K. M. Do, H. T. D. Nguyen, H. Van Mai, T. L. D. Danh, D. Q. Tran and H. Morita, *Tetrahedron*, 2021, **98**, 132426; (*b*) S. Y. Abbas, K. A. M. El-Bayouki and W. M. Basyouni, *Synth. Commun.*, 2016, **46**, 993–1035; (*c*) Z. Tashrifi, M. Mohammadi-Khanaposhtani, M. Biglar, B. Larijani and M. Mahdavi, *Curr. Org. Chem.*, 2019, **23**, 1090–1130.

18 (*a*) J. A. Bleda, P. M. Fresneda, R. Orenes and P. Molina, *Eur. J. Org. Chem.*, 2009, **4**, 2490–2504; (*b*) X. Yang, M. Wu, S. Sun, M. Ding and J. Xie, *J. Heterocycl. Chem.*, 2008, **45**, 1365–1369; (*c*) C. Xie, H. X. Li, M. G. Liu and M. W. Ding, *Chin. Chem. Lett.*, 2008, **19**, 505–508; (*d*) M. M. Vögtle and A. L. Marzinzik, *QSAR Comb. Sci.*, 2004, **23**, 440–459.

19 (*a*) M. Sharif, *Appl. Sci.*, 2020, **10**, 2815; (*b*) M. Abdullaha, S. Mohammed, M. Ali, A. Kumar, R. A. Vishwakarma and S. B. Bharate, *J. Org. Chem.*, 2019, **84**, 5129–5140; (*c*) Q. H. Teng, Y. Sun, Y. Yao, H. T. Tang, J. R. Li and Y. M. Pan, *ChemElectroChem*, 2019, **6**, 3120–3124; (*d*) J. An, Y. Wang, Z. Zhang, Z. Zhao, J. Zhang and F. Wang, *Angew. Chem., Int. Ed.*, 2018, **57**, 12308–12312; (*e*) J. Clayden, N. Greeves and S. Warren, *Org. Chem. Front.*, 2012, **58**, 1261.

20 (*a*) A. Philips, D. Raja, A. Arumugam and W. Lin, *Asian J. Org. Chem.*, 2021, **10**, 1795–1800; (*b*) F. Li, L. Lu and P. Liu, *Org. Lett.*, 2016, **18**, 2580–2583; (*c*) P. S. Kerdphon, T. S. Sanghong, J. Chatwichien, V. Choommongkol, P. Rithchumpon and P. Meepowpan, *Eur. J. Org. Chem.*, 2020, 2730–2734; (*d*) S. Balaji, G. Balamurugan, R. Ramesh and D. Semeril, *Organometallics*, 2021, **40**, 725–734; (*e*) S. R. Vemula, D. Kumar and G. R. Cook, *Tetrahedron Lett.*, 2018, **59**, 3801–3805.

21 (*a*) H. Hou, X. Ma, Y. Lin, J. Lin, W. Sun, L. Wang, X. Xu and F. Ke, *RSC Adv.*, 2021, **11**, 17721–17726; (*b*) V. Nomula and S. N. Rao, *Synth. Commun.*, 2021, **51**, 2602–2612.

22 (*a*) X. Liu, H. Fu, Y. Jiang and Y. Zhao, *Angew. Chem., Int. Ed.*, 2009, **48**, 348–351; (*b*) D. Yang, H. Fu, L. Hu, Y. Jiang and Y. Zhao, *J. Comb. Chem.*, 2009, **11**, 653–657; (*c*) T. Liu, C. Zhu, H. Yang and H. Fu, *Adv. Synth. Catal.*, 2012, **354**, 1579–1584; (*d*) L. Xu, Y. Jiang and D. Ma, *Org. Lett.*, 2012, **14**, 1150–1153; (*e*) B. Li, L. Samp, J. Sagal, C. M. Hayward, C. Yang and Z. Zhang, *J. Org. Chem.*, 2013, **78**, 1273–1277.

23 (*a*) B. Ma, Y. Wang, J. Peng and Q. Zhu, *J. Org. Chem.*, 2011, **76**, 6362–6366; (*b*) F. Zeng and H. Alper, *Org. Lett.*, 2010, **12**, 3642–3644; (*c*) F. Zeng and H. Alper, *Org. Lett.*, 2010, **2**, 1188–1191; (*d*) Z. Zheng and H. Alper, *Org. Lett.*, 2008, **10**, 829–832; (*e*) L. He, H. Li, H. Neumann, M. Beller and X. Wu, *Angew. Chem., Int. Ed.*, 2014, **53**, 1420–1424; (*f*) X. F. Wu, L. He, H. Neumann and M. Beller, *Chem.–Eur. J.*, 2013, **19**, 12635–12638; (*g*) S. W. Tao, R. Q. Liu, J. Y. Zhou and Y. M. Zhu, *ChemistrySelect*, 2020, **5**, 7332–7337.

24 (*a*) T. Ghosh, I. Mandal, S. J. Basak and J. Dash, *J. Org. Chem.*, 2021, **86**, 14695–14704; (*b*) H. L. Liu, X. T. Li, H. Z. Tian and X. W. Sun, *Org. Lett.*, 2021, **23**, 4579–4583; (*c*) A. S. Hussen, S. Bagchi and A. Sharma, *ChemistrySelect*, 2019, **4**, 10169–10173; (*d*) D. Cheng, X. Yan, Y. Pu, J. Shen, X. Xu and J. Yan, *Eur. J. Org. Chem.*, 2021, **2021**, 944–950.

25 (*a*) V. Kesternich, M. Pérez-Fehrmann, A. Puelles, I. Brito, A. Cárdenas, M. Bolte and M. López-Rodríguez, *Z. Krystallog.*, 2013, **228**, 383–384; (*b*) M. Pérez-Ferhmann, V. Kesternich, R. Fernández, F. Verdugo, I. Brito, A. Cárdenas and M. Bolte, *Z. Krystallog.*, 2014, **229**, 401–402; (*c*) M. Pérez-Ferhmann, V. Kesternich, R. Fernández, F. Verdugo, I. Brito, A. Cárdenas and M. Bolte, *Z. Krystallog.*, 2014, **229**, 419–420.

26 M. F. Zayed, H. E. A. Ahmed, A. S. M. Omar, A. S. Abdelrahim and K. El-Adl, *Med. Chem. Res.*, 2013, **22**, 5823–5831.

27 Y. Wang, C. A. Mathis, G. F. Huang, M. L. Debnath, D. P. Holt, L. Shao and W. E. Klunk, *J. Mol. Neurosci.*, 2003, **20**, 255–260.

28 (*a*) V. G. Ugale, H. M. Patel, S. G. Wadodkar, S. B. Bari, A. A. Shirkhedkar and S. J. Surana, *Eur. J. Med. Chem.*, 2012, **53**, 107–113; (*b*) C. Parkanyi and D. S. Schmidt, *J. Heterocycl. Chem.*, 2000, **37**, 725–729.

29 (*a*) R. Chinchilla and C. Nájera, *Chem. Soc. Rev.*, 2011, **40**, 5084–5121; (*b*) R. Dorel, C. P. Grugel and A. M. Haydl, *Angew. Chem., Int. Ed.*, 2019, **58**, 17118–17129; (*c*) P. Ruiz-Castillo and S. L. Buchwald, *Chem. Rev.*, 2016, **116**, 12564–12649; (*d*) S. E. Hooshmand, B. Heidari, R. Sedghi and R. S. Varma, *Green Chem.*, 2019, **21**, 381–405; (*e*) J. P. Knowles and A. Whiting, *Org. Biomol. Chem.*, 2007, **5**, 31–44; (*f*) F. Christoffel and T. R. Ward, *Catal. Lett.*, 2018, **148**, 489–511.

30 (*a*) X. Liu, H. Fu, Y. Jiang and Y. Zhao, *Angew. Chem., Int. Ed.*, 2009, **48**, 348–351; (*b*) C. Bingi, K. Y. Kola, A. Kale, J. B. Nanubolu and K. Atmakur, *Tetrahedron Lett.*, 2017, **58**, 1071–1074; (*c*) J. F. Liu, J. Lee, A. M. Dalton, G. Bi, L. Yu, C. M. Baldino, E. McElory and M. Brown, *Tetrahedron Lett.*, 2005, **46**, 1241–1244; (*d*) M. Sharif, J. Opalach, P. Langer, M. Beller and X. F. Wu, *RSC Adv.*, 2014, **4**, 8–17.

31 (*a*) H. W. Grimmel, A. Guenther and J. F. Morgan, *J. Am. Chem. Soc.*, 1946, **68**, 542–543; (*b*) S. Xue, J. Mckenna, W. Shieh and O. Repic, *J. Org. Chem.*, 2004, **69**, 6474–6477.

32 T. Mosmann, *J. Immunol. Methods*, 1983, **65**, 55–63.

33 M. V. Raimondi, O. Randazzo, M. La Franca, G. Barone, E. Vignoni, D. Rossi and S. Collina, *Molecules*, 2019, **24**, 1–19.

34 J. R. Bertino, *Best Pract. Res., Clin. Haematol.*, 2009, **22**, 577–582.

35 E. Ercikan-Abali, H. Celikkaya, Y.-C. Hsieh, D. Banerjee and J. R. Bertino, *Curr. Enzyme Inhib.*, 2012, **8**, 107–117.

36 G. Bhabha, D. C. Ekiert, M. Jennewein, C. M. Zmasek, L. M. Tuttle, G. Kroon, H. J. Dyson, A. Godzik, I. A. Wilson and P. E. Wright, *Nat. Struct. Mol. Biol.*, 2013, **20**, 1243–1249.

37 P. Pathak, P. K. Shukla, V. Kumar, A. Kumar and A. Verma, *Inflammopharmacology*, 2018, **26**, 1441–1453.

38 (*a*) R. D. Cramer, D. E. Patterson and J. D. Bunce, *J. Am. Chem. Soc.*, 1988, **110**, 5959–5967; (*b*) M. Clark, R. D. Cramer, D. M. Jones, D. E. Patterson and P. E. Simeroth, *Tetrahedron Comput. Methodol.*, 1990, **3**, 47–59.

39 A. Daina, O. Michielin and V. Zoete, *J. Chem. Inf. Model.*, 2014, **54**, 3284–3301.

40 T. Cheng, Y. Zhao, X. Li, F. Lin, Y. Xu, X. Zhang, Y. Li, R. Wang and L. Lai, *J. Chem. Inf. Model.*, 2007, **47**, 2140–2148.

41 Y. M. Ikuo Moriguchi, Shuichi Hirono, Qian Liu and Izumi Nakagome, *Chem. Pharm. Bull.*, 1992, 127–130.

42 J. S. Delaney, *J. Chem. Inf. Comput. Sci.*, 2004, **44**, 1000–1005.

43 J. Ali, P. Camilleri, M. B. Brown, A. J. Hutt and S. B. Kirton, *J. Chem. Inf. Model.*, 2012, **52**, 2950–2957.

44 N. M. O'Boyle, M. Banck, C. A. James, C. Morley, T. Vandermeersch and G. R. Hutchison, *J. Cheminform.*, 2011, **3**, 1–14.

45 *QUACPAC 2.0.1.2: OpenEye Scientific Software*, Santa Fe, NM, **https://www.eyesopen.com**.

46 P. C. D. Hawkins, A. G. Skillman, G. L. Warren, B. A. Ellingson and M. T. Stahl, *J. Chem. Inf. Model.*, 2010, **50**, 572–584.

47 M. McGann, *J. Chem. Inf. Model.*, 2011, **51**, 578–596.

48 *SZYBKI 1.10.1.2: OpenEye Scientific Software*, Santa Fe, NM, **https://www.eyesopen.com**.

49 P. Tosco and T. Balle, *J. Mol. Model.*, 2011, **17**, 201–208.

50 A. Daina, O. Michielin and V. Zoete, *Sci. Rep.*, 2017, **7**, 42717.